Thin Solid Films 520 (2012) 4394–4401

Contents lists available at SciVerse ScienceDirect

Thin Solid Films

journal homepage: www.elsevier.com/locate/tsf

Influence of high temperature processing of sol–gel derived barium titanate thin films deposited on platinum and strontium ruthenate coated silicon wafers

Tomasz M. Stawski, Wouter J.C. Vijselaar, Ole F. Göbel [1], Sjoerd A. Veldhuis, Brian F. Smith, Dave H.A. Blank, Johan E. ten Elshof *

MESA+ Institute for Nanotechnology, University of Twente, P.O. Box 217, 7500 AE Enschede, The Netherlands

ARTICLE INFO

Article history:
Received 14 September 2011
Received in revised form 11 January 2012
Accepted 6 February 2012
Available online 12 February 2012

Keywords:
Films
Interfaces
Sol–gel processes
$BaTiO_3$
$SrRuO_3$
Dielectric properties

ABSTRACT

Thin films of barium titanate (BTO) of 200 nm thickness, derived from an alkoxide–carboxylate sol–gel process, were deposited on Pt/Ti and $SrRuO_3/ZrO_2$–8%Y_2O_3 coated Si wafers. Films with a dense columnar microstructure were obtained by repeated deposition of thin amorphous layers from low-concentrated sols, and crystallization at 800 °C. This method added 10 nm thickness to the crystalline BTO film in each deposition step. The harsh processing conditions had a negative impact on the platinized silicon wafers, where Pt–Si silicides were formed. This led to diffusion of Si into BTO and interfacial silicate formation. The interfacial silicate layer was the cause of deteriorated dielectric and ferroelectric properties of the BTO layer. Use of $SrRuO_3/ZrO_2$–8%Y_2O_3/Si substrates solved the problem. No diffusion of Si was observed, and BTO films with good dielectric and ferroelectric properties were obtained.

© 2012 Elsevier B.V. All rights reserved.

1. Introduction

Barium titanate ($BaTiO_3$; BTO) is a widely used high-*k* ceramic dielectric material. It is utilized in a wide range of applications, many of which are based on the use of BTO thin films. BTO is an important dielectric material, for instance in commercial multi-layer ceramic capacitors. The minimum $BaTiO_3$ layer thickness that can be achieved with state of the art tape casting methods is about 1 μm. Barium titanate is used in crystalline form, which implies the use of starting powders with a particle size of *ca.* 200 nm [1]. Further reduction of the barium titanate layer thickness requires finer powders obtained by improved synthesis and deposition techniques. One of the feasible alternatives is the deposition of amorphous precursors of barium titanate and their further reaction and crystallization to a perovskite phase [2]. Good control and understanding of the process in all stages is required to obtain a film with desired electrical and morphological properties. This can be achieved by wet-chemical processing methods. Moreover, as the wet-chemical methods are based on liquid precursors, direct deposition of precursor thin films onto substrates by means of spin-casting, deep-casting or misted source deposition, followed by pyrolysis and crystallization is possible [2–5]. These off-contact deposition techniques enable direct fabrication of thin films of $BaTiO_3$ on bare silicon and electrode-coated silicon wafers. It opens up the possibility to integrate inexpensive chemically derived barium titanate with silicon technology, *e.g.* as dielectric material for dynamic random access memory (DRAM) [6] and non-volatile ferroelectric memories [7]. It has been demonstrated that chemically fabricated thin films of $BaTiO_3$ yield very good dielectric properties, with relative permittivities > 600 at a layer thickness < 200 nm [8,9]. Use of oxides with high dielectric constant for DRAM applications would enable fabrication of high-capacity memory chips using simple planar capacitor geometries, instead of the currently used complicated trench of stacked capacitors with SiO_2 ultra-thin (< 4 nm) films. This would simplify the production process significantly, and reduce costs [6].

Among the synthesis methods the sol–gel process, in particular the alkoxide–carboxylate synthesis, the double alkoxide synthesis, the micro-emulsion synthesis, and the precipitation methods (alkoxide–hydroxide sol precipitation) received much attention [2]. The alkoxide–carboxylate was employed widely for $BaTiO_3$ synthesis since the first reports [10].

In order to obtain a barium titanate thin film of desired electrical properties a number of factors have to be taken into account, among which thermal processing plays probably the most important role [3,4,11]. The heat treatment can be divided into several stages [12]: (1) removal of residual solvents, T < 200 °C; (2) pyrolysis of organic moieties, T = 250–500 °C, (3) onset of perovskite phase crystallization, thermal decomposition of residual carbonates, T = 600–800 °C; (4) sintering, T > 800 °C. According to Mosset et al., barium carbonate and titanium dioxide are formed after pyrolysis and form $BaTiO_3$ above 650 °C [13]. A number of intermediate phases have been suggested in literature, such as $Ba_2Ti_2O_5CO_3$ [2,12]. The crucial point in the syntheses is

* Corresponding author. Tel.: +31 53 489 2695; fax: +31 53 489 2990.
E-mail address: j.e.tenelshof@utwente.nl (J.E. ten Elshof).
[1] Present address: Bruker Nano, Dynamostraße 19, 68165 Mannheim, Germany.

0040-6090/$ – see front matter © 2012 Elsevier B.V. All rights reserved.
doi:10.1016/j.tsf.2012.02.029

that temperatures > 650 °C are essential for this phase to decompose and for barium titanate to crystallize.

The heating protocol can be a one- or a two-step procedure. In the latter case, the as-deposited film is initially processed at a pyrolysis temperature < 500 °C, and then heated to 850 °C at a rate of 1 °C/min, yielding relatively dense barium titanate [3,8,9]. In the one-step process a dried xero-gel film is placed in an oven preheated at *ca*. 850 °C. At this temperature the rate of pyrolysis is orders of magnitude higher than below 500 °C [3,14]. The thin film density is improved by delaying the onset of crystallization to that of higher temperatures, thereby reducing the number of nucleation events and yielding larger grains [3,8]. It was demonstrated that one-step processing yielded films with better dielectric properties than two-step processing [8,9]. One-step processed films were denser and had larger grains than films obtained from a two-step process.

The highest reported permittivity values for sol–gel derived barium titanate films with a thickness < 200 nm on Pt electrodes were measured for BTO with a columnar microstructure [8,9]. Barium titanate is known to nucleate homogenously, yielding films of grainy microstructure [3,4,11]. In order to nucleate the perovskite phase heterogeneously, it must be deposited in a sequence of very thin layers, with a heat-treatment at 700–800 °C after each deposition step. This is done by spincasting sol–gel precursors of very low concentration, typically < 0.2 mol/dm^3 for barium titanate or barium strontium titanate from alkoxide–carboxylate precursors [9]. Each cycle adds typically 10–20 nm to the total thickness of the film. The films have a high relative density, close to 100%, and high relative permittivities, typically above 600, when annealed at 800 °C.

The method of production exposes the film to extreme conditions, such as fast cooling and heating, and high temperature, which may be a problem when silicon-based substrates are used. TiO_2 is unstable in contact with silicon > 700 °C, whereas $SrTiO_3$ was demonstrated to react with Si at temperatures as low as 200–600 °C [15].

It was the purpose of this work to investigate the formation of barium titanate thin films on Pt/Ti/SiO_2/Si and $SrRuO_3$/ZrO_2–8%Y_2O_3/SiO_2/Si substrates. We investigated the formation of interfacial phases from one-step processed sol–gel derived columnar barium titanate thin films. Field-emission scanning electron microscopy (FE-SEM), X-ray powder diffraction (XRD), and depth-resolved X-ray photoelectron spectroscopy (XPS) were used for structural analysis.

2. Experimental details

2.1. Synthesis of barium titanate (BTO) precursor sols

Barium acetate (> 99%, Riedel-deHaën) and titanium(IV) *iso*-propoxide (99.999%, Sigma-Aldrich) were used as precursor materials. Glacial acetic acid (99.8%, Acros) and 2-methoxyethanol (> 99.3%, Sigma-Aldrich) were used as solvents, stabilizers, and chelating agents. Two stock solutions were made. A Ba-acetate solution was prepared by dissolving barium acetate in acetic acid and subsequent refluxing at 105 °C for 8 h to remove all remaining water. The final concentration was adjusted to 1.0 mol/dm^3. The second stock solution was based on titanium *iso*-propoxide with 2-methoxyethanol as solvent, yielding a precursor concentration of 1.0 mol/dm^3. It was stirred in a glove box under nitrogen atmosphere. Both stock solutions were stirred at room temperature for 24 h. They were then stored at room temperature. Prior to the experiments, the stock solutions were mixed in 1:1 molar ratios and stirred for 5 min, yielding a concentration of 0.50 mol/dm^3 in the final BTO precursor solution. In the next step they were diluted with 2-methoxyethanol to reach a concentration of 0.1 mol/dm^3 in the final BTO precursor solution.

2.2. Thin film fabrication

BTO precursor sols of 0.1 mol/dm^3 were spin-cast (Laurell WS-400B-6NPP-Lite spincoater) onto 1 × 1 cm^2 substrates at 3000 rpm for 40 s. The as-prepared films were dried on a hot-stage at 100 °C for 15 min. In subsequent steps, substrates with BTO films were placed in a pre-heated oven (Milestone PyroPrep) at 800 °C for 5 min, then quenched to room temperature and used as substrate for the next layer of BTO sol. The process was repeated several times, typically 20. Two kinds of substrates were investigated:

(1) Si(001) with native SiO_2, a Ti adhesion layer of 40 nm thickness, and a 200 nm thick Pt electrode. This substrate is further referred to as Si/Ti/Pt;
(2) Si(001) with native SiO_2, a 70 nm thick buffer layer of yttrium stabilized zirconia (YSZO), and a 200 nm thick $SrRuO_3$ electrode. This substrate is further referred to as Si/YSZO/SRO.

The Si/Ti/Pt substrates were made by sputtering (Sputterke, DC sputter system, $p_{Ar} = 0.66$ Pa, $T = 25$ °C), and the Si/YSZO/SRO substrates were manufactured by pulsed laser deposition using a KrF excimer laser, as described elsewhere [16,17]. Typically, several monolayers of YSZO buffer were grown under argon instead of oxygen atmosphere ($p_{Ar} = 2$ Pa, $T = 850$ °C). This step enabled scavenging of native silicon oxide by reduced Zr and Y, and provided a basis for coherent and epitaxial growth of YSZO in an oxygen atmosphere ($p_{O2} = 2$ Pa, $T = 850$ °C) without HF processing of Si [17,18]. SRO was deposited at $p_{O2} = 13$ Pa, $T = 650$ °C. By this means, oriented metallic conductive substrates SRO(110)/YSZO(001)/Si(001) were obtained [17].

2.3. Thin film characterization

Selected samples were broken with pliers and the cross-section was analyzed by FE-SEM (0.5–2.0 keV, Zeiss 1550) to determine layer thickness and film microstructure. XRD patterns of films were measured on a diffractometer with Cu anode and Ni filter for Cu K_β radiation (Philips PW1830). Patterns were measured in a continuous ω-2θ mode with 0.02° step size and counting time 5 s.

XPS spectra were recorded to determine the elemental surface composition (Physical Electronics Quantera SXM, Al K_α 1486.6 eV). Depth profiles were recorded with an Ar^+ beam of 3 kV, rastering an area of 9 mm^2 using Zalar rotation to avoid shadowing effects of the sputter beam. Due to the unknown sputtering rate of Ar^+, we cannot directly correlate elemental composition to a specific depth under the surface of the film. The surface of the samples was sputtered away by removing in each step approximately 5–20 nm thickness of the film, and the XPS spectra were being collected afterwards, yielding information about the surface elemental composition as a function of total sputter time. Total counting time per element was 5 min. Data reduction was performed by means of Multipak 8.0 software. Fitting of spectra was done by shifting the measured spectra with respect to known reference binding energies (BE): aliphatic carbon C 1*s* at 284.8 eV or gold Au 4$f_{7/2}$ at 83.96 eV, silver Ag 3$d_{5/2}$ at 368.21 eV and copper Cu 2$p_{3/2}$ at 932.62 eV. Specific elements and their characteristic chemical shifts were identified by comparing measured spectra with information contained in the NIST Database for the Simulation of Electron Spectra for Surface Analysis ver. 1.1 [19] and other references available in literature.

Gold–palladium electrodes were sputtered on the top surface of selected films (95% Au–5% Pd, Polaron SC7640, $p_{Ar} = 1$ Pa, $T = 30$ °C) through a silicon micro-machined shadow mask, with a good contact between the film and the mask. The area of the electrode was 1.0 mm^2 ± 0.04% and the thickness was 100 nm. Films with deposited top electrodes were post-annealed at 350 °C for 1 h to improve adhesion of the electrodes to the surface. The capacity as a function of applied voltage measurement (*C*–*V*) of as-prepared capacitors was

carried out in a top-to-bottom configuration at 500 kHz at room temperature, with a bias of −5 V to +5 V and AC voltage of 1 V (Karl Suss PM8 low-leakage Manual Probe Station). The dielectric constant was extracted using the plate capacitor equation, with a dielectric layer averaged-thickness obtained from FE-SEM characterization.

Local piezoresponse force microscopy (PFM) loops were obtained using a Bruker Dimension Icon atomic force microscope with a conducting Cr/Pt coated silicon probe with a resonance frequency of 75 kHz and a force constant of 3 N/m. The DC voltage was ramped from +10 V to −10 V and back to +10 V with a ramp frequency of 0.05 Hz. The AC probe voltage used to measure the piezoresonse during the DC ramp was 5 V at a frequency of 350 kHz.

2.4. Reaction of BTO with amorphous SiO_2

High temperature XRD (Philips X'Pert MPD, Anton-Paar HTK16 high-temperature chamber, Cu anode and Ni filter for Cu K_β radiation) was used to study phases that formed in the reaction between barium titanate and silicon. Patterns were measured in a continuous mode with 0.04° step size and 15 s counting time. The as-synthesized powder of nano-crystalline barium titanate (particle diameter < 10 nm) prepared following the recipe in ref. [20] was thoroughly mixed in a mortar with 10 wt.% fine amorphous SiO_2 powder (Sigma-Aldrich), and placed on a Pt heater in the high-temperature chamber. XRD patterns were collected at selected temperatures ranging from 200 °C to 850 °C, with a typical dwell time of 20 h at a given temperature. This ensured that samples were always in thermal equilibrium.

3. Results and Discussion

3.1. FE-SEM and XRD analysis

Fig. 1 presents the FE-SEM pictures of cross-sections of BTO thin films on Si/YSZO/SRO and Si/Ti/Pt. The corresponding BTO layer thicknesses were 208 nm ± 2% and 201 nm ± 2%, respectively. The same number of deposition steps was used to fabricate the two films. A dense columnar structure is visible, indicating that one-step thermal treatment combined with multi-step deposition yielded the desired microstructure. The inset in Fig. 1A illustrates the linear dependence between the number of deposited layers and the final thickness of the thermally processed film. In the film fabricated on a Si/YSZO/SRO substrate, all the expected phases can be distinguished by FE-SEM: Si substrate, *ca.* 70 nm of dense YSZO and *ca.* 200 nm of dense SRO electrode, underneath the barium titanate film (Fig. 1A). No interfacial phases can be observed, as confirmed by XRD in Fig. 2A, where $BaTiO_3$, $SrRuO_3$, and YSZO are present. The preferential (001) orientation of YSZO can be concluded from the presence of only (200) and (400) peaks in the XRD pattern. The coherence was further extended to the SRO film, which exhibited only (110) and (220) peaks in XRD. Making a clear distinction between tetragonal and cubic barium titanate was not possible due to peak broadening caused by the small grain size. Furthermore, the BTO film was (110) oriented, as suggested by the strongly increased relative intensity of the peak in the proximity of 2θ ~ 31°, and the clear indication from the rocking curve (full-width-at-half-maximum, FWHM = 1.8°) of the BTO (110) peak (figure not shown).

In the BTO film deposited on Si/Ti/Pt, no individually distinguishable Ti or Pt layer was present. Instead, a single dense layer of 200 nm thickness had formed. Barium titanate was also present in the film, Fig. 2B. Moreover, a number of strong unidentified peaks, and a peak of Si (100) at 2θ = 69.2° (004) were recognized. Some of the peaks coincided with BTO peaks, like the one at 2θ ~ 56°. An interfacial phase of 20 nm thickness formed between the barium titanate thin layer and the Pt electrode (Fig. 1B).

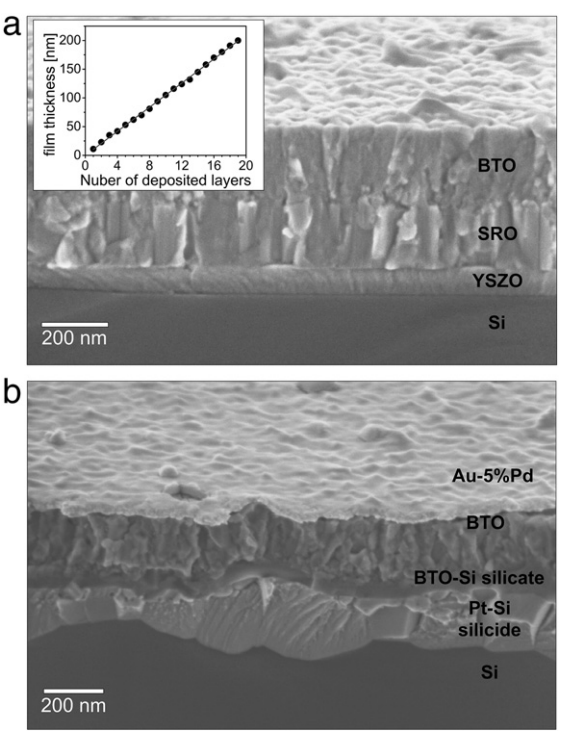

Fig. 1. FE-SEM images of cross-sections of films of barium titanate fabricated by multi-layer deposition and processed by one-step annealing at 800 °C. a) BTO/SRO/YSZO/Si film; b) BTO/Pt/Ti/Si film. Inset shows the dependence between number of deposition steps and BTO layer thickness.

3.2. Depth-resolved XPS analysis

Elemental composition as a function depth into both types of thin films was determined by depth-resolved XPS analysis. In the case of BTO on Pt/Ti/Si, survey scans from 1345 eV to 5 eV with dE = 0.8 eV in three cycles demonstrated clearly that only Ti, Ba and O were present at the sample surface. Scans with depth profiling were

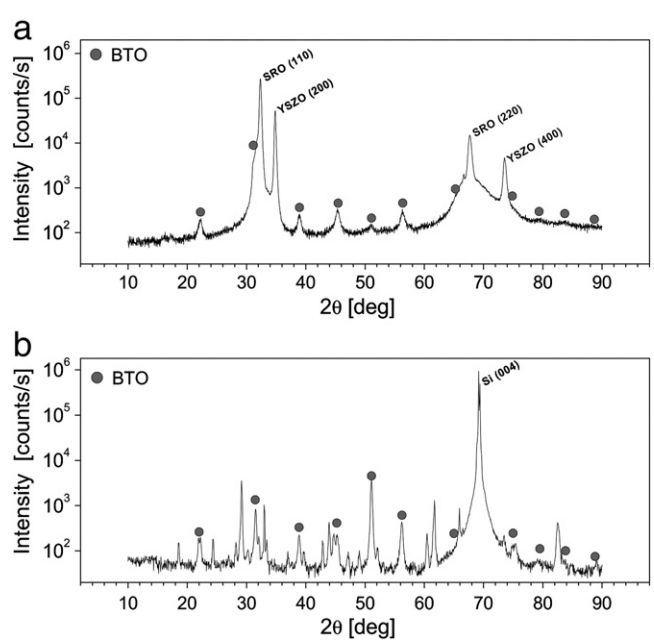

Fig. 2. XRD patterns of films of barium titanate fabricated by multi-layer deposition and processed by one-step annealing at 800 °C. a) BTO/SRO/YSZO/Si; b) BTO/Pt/Ti/Si. A number of unmarked diffraction peaks from silicate and silicide phases are present. BTO peaks are marked by a symbol.

performed in the selected binding energy ranges of all present elements, *i.e.* Pt 4*f*; Si 2*p*; Ti 2*p*; O 1*s*; Ba $3d_{5/2}$. Atomic concentrations as a function of sputter time are shown in Fig. 3A. The concentrations are based on the peak areas and the relative sensitivity factors.

While Ar^+ sputtering does not provide direct information on the sputtering depth, Fig. 3A shows clearly that stoichiometric $BaTiO_3$ was present in the film during 25 min of sputtering. This means that the barium titanate layer was sputtered at a rate of 8 nm/min. The high concentration of Si at the top surface is an artifact from the measurement, caused by shake-up peak of Ba 4*d*. A real Si signal was present after $t = 25$–40 min, indicating an increasing silicon concentration with depth. At $t = 40$ min a Pt 4*f* signal appeared, which reached 50 at.% by the end of the sputtering process. The Si concentration was *ca.* 40 at.% at the same depth. Peak analysis of the Si 2*p* spectrum showed that Si was present in two oxidation states, namely Si^{4+} with a BE of 108 eV [21] at $t = 25$–40 min, and Si^0 with a BE of 100 eV [21,22] at $t > 40$ min, Fig. 3B. The chemical shift of Pt 4*f* over the whole investigated depth range is typical for PtSi or Pt_2Si, Fig. 3C [22]. At $t < 40$ min, the Ba concentration was approximately two times higher than the Ti concentration, and at $t \sim 40$ min, the concentrations of Ba and Ti were close to 0 and 5 at.%, respectively. The chemical shift of Ti suggested that it was present in oxidized form [23] (Fig. 3D). Analysis of O 1*s* depth-resolved spectra showed that the oxygen concentration remained constant until $t = 25$ min, after which it decreased substantially until $t = 40$ min (Fig. 3). Until $t = 25$ min the chemical shift of O 1*s* corresponded to the one found for barium titanate, *i.e.* BE = 527.5 eV [24]. At $t > 25$ min, the chemical shifts were attributed to two Si/O stoichiometries: SiO at $t = 25$–40 min with BE = 529.0 eV [25], followed by SiO_2 at $t > 40$ min with BE = 531.7 eV [21].

The following film morphology can be deduced from these data. Stoichiometric barium titanate forms a layer of ~200 nm thickness. Beneath that, a 20 nm thick interfacial silicate layer composed of Ba,

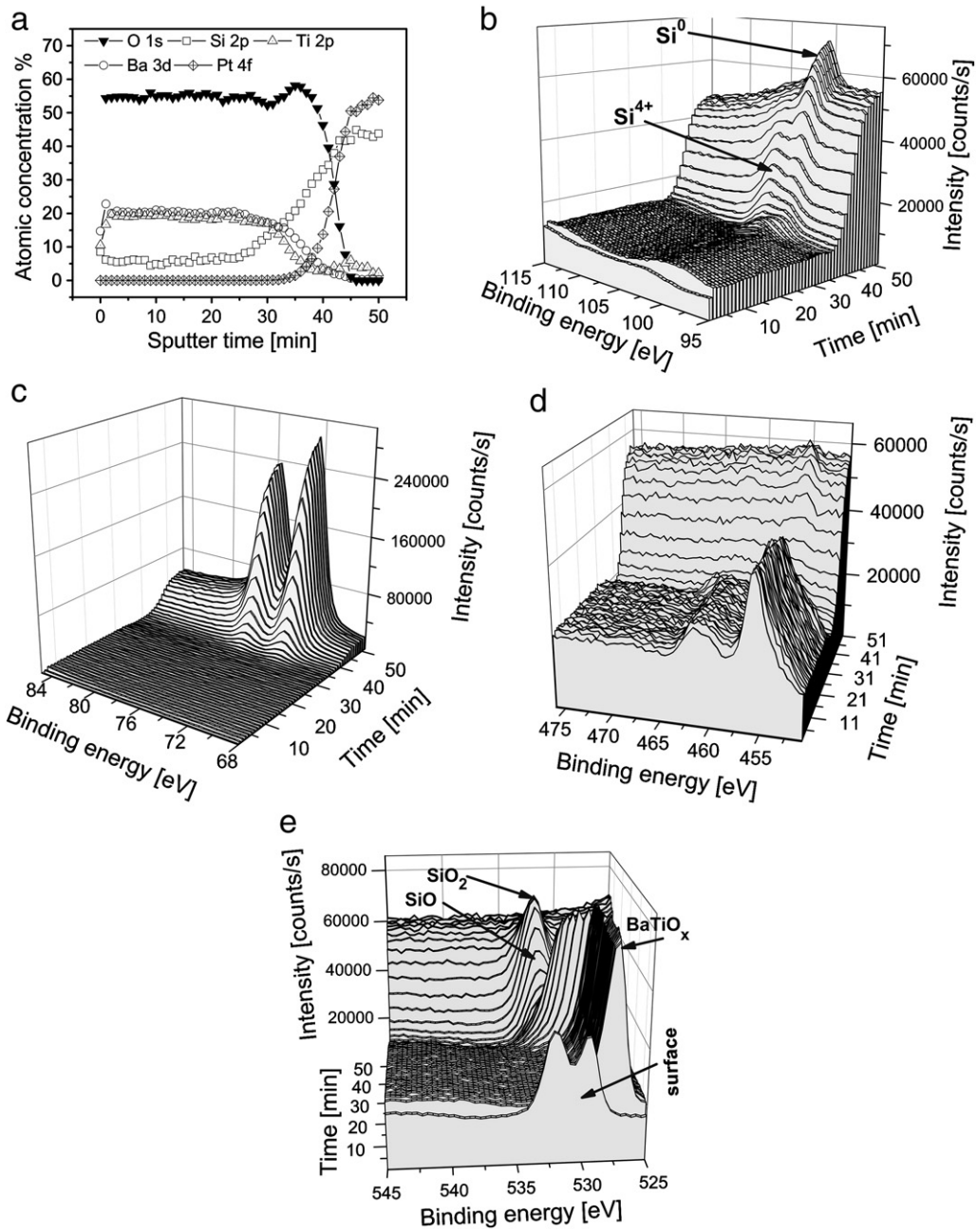

Fig. 3. XPS depth profile of 200 nm barium titanate film on Pt/Ti/Si. a) Atomic concentrations in film as function of sputter time. XPS spectra shown: b) Si 2*p*; c) Pt 4*f*; d) Ti 2*p*; e) O 1*s*. Sputter rate is approximately 8 nm/min for BTO.

Ti, Si, and O was formed. The detected silicate phase may correspond to fresnoite, $Ba_2Ti(Si_2O_7)O$, at t~38 min. Considering the varying concentrations of Si and O, a diffusion mechanism is proposed to explain silicate interface formation. Thus, other stoichiometries than fresnoite were probably also present. Beyond the interfacial layer, at the position of the Pt/Ti/Si electrode, a silicide phase with gross composition 50 at.% Pt–40 at.% Si, and very small concentrations of Ti and O were detected.

The question is if the observed interfacial layer formed as a result of the repeated cooling and annealing cycles, *i.e.* 20 cycles of 5 min at 800 °C and back to room temperature, in the barium titanate film formation process, or if it started directly at the beginning of the process, when the first layer of barium titanate was deposited. To answer this question, a 20–25 nm barium titanate film was made via deposition in two layers. The annealing time at 800 °C was reduced to 60 s. Survey scans (not shown here) from 1345 eV to 5 eV with dE = 0.8 eV in 3 cycles demonstrated clearly that not only Ti, Ba and O were present at the sample surface, but also Si. The depth-resolved elemental composition is shown in Fig. 4A. The sputter Ar^+ rate that was in the barium titanate layer was approximately 4–5 nm/min. Ba and Ti remained in a near-stoichiometric ratio until $t = 5$ min. Then the Ba concentration dropped to 0, and Ti remained at a constant level of 5 at.% until $t = 12$ min. A non-negligible signal of Si was present in the material from the surface, and its concentration reached 40 at.% at $t = 5$ min. Similarly, a Pt 4*f* signal that corresponds to a concentration of ~50 at.% was detected from $t = 5$ min onwards. Pt formed a silicide phase over the whole thickness of the electrode. Si was present in two oxidation states (Fig. 4B), with Si^{4+} at a depth corresponding to the location of the interface between BTO and Pt electrode. This shows undoubtedly that Si diffusion to the barium titanate precursor film occurs very fast at a temperature of 800 °C, and silicate formation occurs from the very beginning of the process. On the other hand, Pt does not diffuse into the BTO or interfacial layer. The results can be rationalized by considering the semi-amorphous character of the barium titanate precursor sol, and the low stability of TiO_2 in contact with Si and silicide phases at the processing temperature [15].

XPS analysis with depth profiling was also performed on a BTO/SRO/YSZO/Si film. Here, Si 2*p*; Y 3*d*; Zr 3*d*; Sr 3*d*; Ru $3p_{3/2}$ and 3*d*; Ti 2*p*; O 1*s*; Ba $3d_{5/2}$ spectra were measured. A 200 nm thick film of barium titanate prepared in 20 deposition and calcination steps was analyzed. The measurement clearly showed that well-defined layers were present in the stack (Fig. 5A). In the first 20 min of the sputter process only stoichiometric $BaTiO_3$ was present. At $t = 22$–26 min an interface containing Ru, Ti, Ba and Sr was detected. The XPS spectra of Ru $3p_{3/2}$ overlap with a part of the Ti $2p_{3/2}$ peak until $t = 24$ min (Fig. 5B).

The stoichiometry of the SRO layer was established on the basis of the Ru $3p_{3/2}$ peak, because Ru 3*d* coincides with Sr $3p_{1/2}$ around 280 eV [26–29]. The positions of the Sr and Ru peaks remained constant at $t = 32$–56 min (Fig. 5B–D), suggesting a constant composition. The layer contained 20 at.% Ru–30 at.% Sr–50 at.% O, *i.e.* a stoichiometry that differs from $SrRuO_3$. The Ru 3*d* and $3p_{3/2}$ peaks were clearly asymmetric, indicating the presence of nonequivalent Ru atoms or multiplet splittings in metallic SRO caused by correlated electron behavior [26,28] (Fig. 5). The binding energy of Ru $3d_{5/2}$ at 280.3 eV indicated that this element was present in the form found in RuO_2 or Ru^0 [29–31]. The stoichiometry of the film suggests that a Sr-rich ruthenate phase may have formed upon annealing, when part of Ru^{4+} was oxidized to gaseous RuO_4 or RuO_3 [27]. Indeed, a small maximum at 282.2 eV at $t = 26$–28 min (Fig. 5C) may possibly be attributed to RuO_3 [30,31]. The O 1*s* spectrum showed an oxygen peak at a single BE = 529.4 eV throughout the whole SRO film. This binding energy is typical for RuO_2, SrO and for $SrTiO_3$ surfaces [30,31]. Its symmetric, non-split shape clearly indicated that only one form of oxygen was present in the film. This excluded, for instance, the presence of OH^- [32]. The Sr $3d_{5/2}$ spectrum is shown in Fig. 5D. Two closely localized peaks at BE = 132.4 eV and BE = 134.0 eV can be distinguished and they remain unchanged at $t = 32$–56 min. These binding energies are in good agreement with the binding energies of $SrTiO_3$, while they differ from values typically found for pure SrO (132.6 eV and 135.3 eV) [32]. It indicates that Sr has a slightly different chemical environment in SRO than in pure SrO. Hence, the presence of a Sr-rich ruthenate phase seems very likely. Its stoichiometry is difficult to assess, but considering the thermodynamic requirements for the co-existence of phases, $SrRuO_3$, Sr_2RuO_4, and/or $Sr_3Ru_2O_7$ are possible, because $SrRuO_3$ and SrO cannot co-exist [26]. We compared these spectra with those of an unprocessed SRO/YSZO/Si surface. Several nanometers deep into a fresh SRO film the composition 30 at.% Sr–30 at.% Ru–40 at.% O was found. Therefore, it is evident that part of the Ru was lost upon addition and heat treatment of the BTO layer.

After $t = 55$ min the YSZO layer of general composition 35 at.% Zr–6 at.% Y–59 at.% O was reached. A sharp interface was detected between the YSZO and SRO layers, showing that no intermixing between these two phases occurred (insets in Fig. 5C and D). After 90 min of sputtering only metallic Si^0 was present.

3.3. Formation of Ba–Ti-silicate phase

The formation of silicate was investigated by high temperature XRD using a model system of 90 wt.% BTO nano-powder mixed and 10 wt.% silicon dioxide powder. Fig. 6 shows X-ray diffractograms measured between 200 and 850 °C, with a hold time of 20 h at each temperature. Up to 650 °C only diffraction peaks originating from barium titanate, barium carbonate impurity and the Pt holder were measured. As the temperature was raised to 750 °C, new peaks

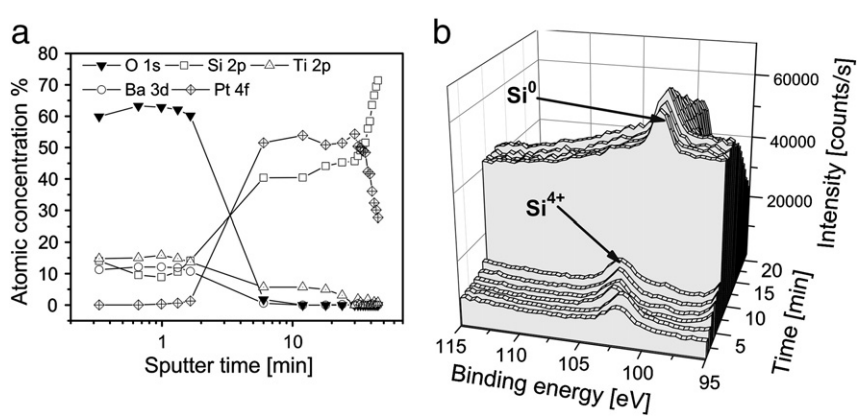

Fig. 4. XPS depth profile of 25 nm barium titanate film on Pt/Ti/Si. a) Atomic concentrations in film as function of sputter time; b) XPS spectra of Si 2*p* region as a function of sputter time. Sputter rate is approximately 4 nm/min for BTO.

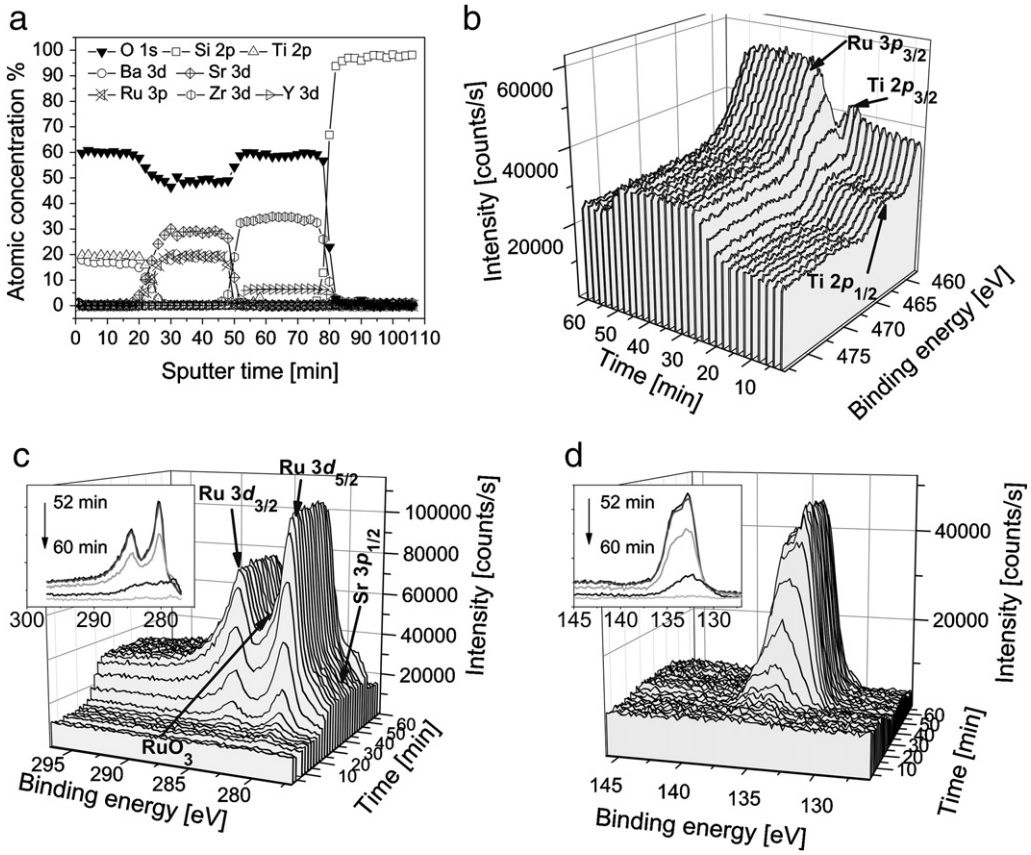

Fig. 5. XPS depth profile of 200 nm barium titanate film on SRO/YSZO/Si. a) Atomic concentrations in film as function of sputter time. XPS spectra shown: b) Ru $3p_{3/2}$ and Ti 2*p* (partially); c) Ru 3*d* and Sr $3p_{1/2}$ (partially); d) Sr 3*d*. Sputter rate is approximately 8 nm/min for BTO. The insets in c and d show the BE curves of Ru and Sr after 52–60 min of sputtering.

were detected. The compound was undoubtedly recognized as fresnoite, $Ba_2Ti(Si_2O_7)O$ [33]. At 850 °C the fresnoite phase showed higher intensity diffraction peaks of lower FWHM. Hence, no reaction between BTO and SiO_2 took place at temperatures up to 650 °C, even when extremely long dwell times were used. This observation illustrates the high stability of barium titanate in contact with Si at this temperature. It is known from literature that crystalline silicate is formed at 730 °C [34].

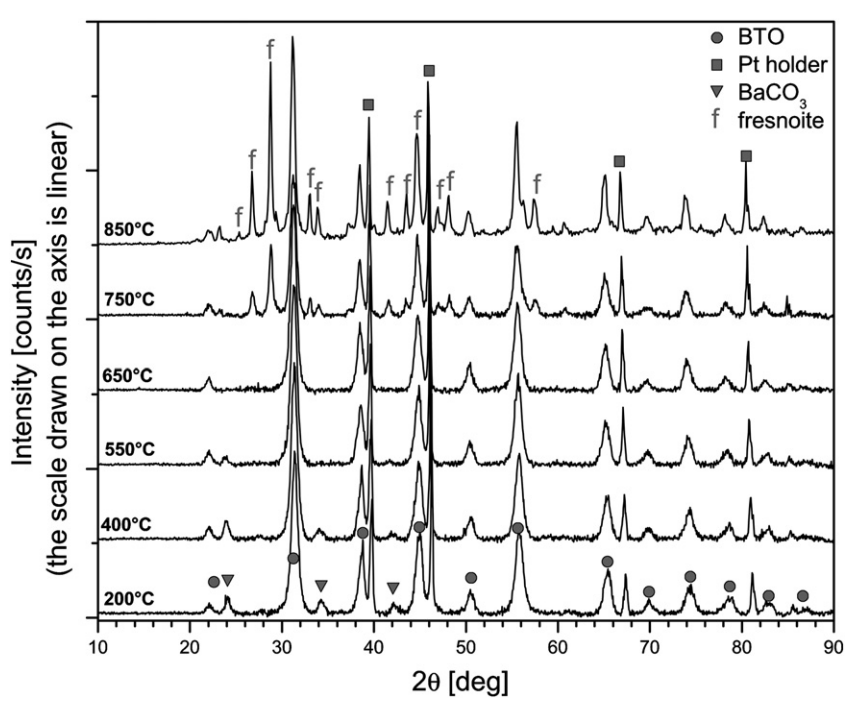

Fig. 6. High temperature XRD patterns of 90 wt.% barium titanate nano-powder mixed with 10 wt.% amorphous SiO_2 powder between 200 and 850 °C, with a typical dwell time of 20 h at all temperatures. Identified phases are marked by symbols.

3.4. Dielectric and ferroelectric properties

C–V measurements were performed on two investigated films, namely BTO/SRO/YSZO/Si and BTO/Pt/Ti/Si. Results are presented in Fig. 7A. The relative permittivities were $\varepsilon_r = 672 \pm 1\%$ for BTO/SRO/YSZO/Si, and $\varepsilon_r = 161 \pm 1\%$ for BTO/Pt/Ti/Si at the peak maximum. In both cases a non-linear dielectric response was measured, yielding the characteristic "butterfly" shape in the *C–V* curve, with two distinguishable maxima of relative permittivity dependent on electric field direction. The shape indicates that the films were ferroelectric. A horizontal shift of the "butterfly" curve relative to 0 V is visible. This can be explained by the fact that the top and bottom electrodes were made of different materials and processed at different temperatures, which results in asymmetric properties of the upper and lower electrode-dielectric interfaces. The effect is discussed further below. The measured relative permittivity value of 670–680 at room temperature on SRO/YSZO/SI is comparable to values found for other sol–gel derived BTO thin films [3,8,9]. The high value of ε at 500 kHz suggests that BTO may be applicable in DRAMs, where good high-frequency performance is required [6]. The YSZO buffer layer is crucial to prevent diffusion of Si to the SRO electrode and the dielectric phase [15,17,18].

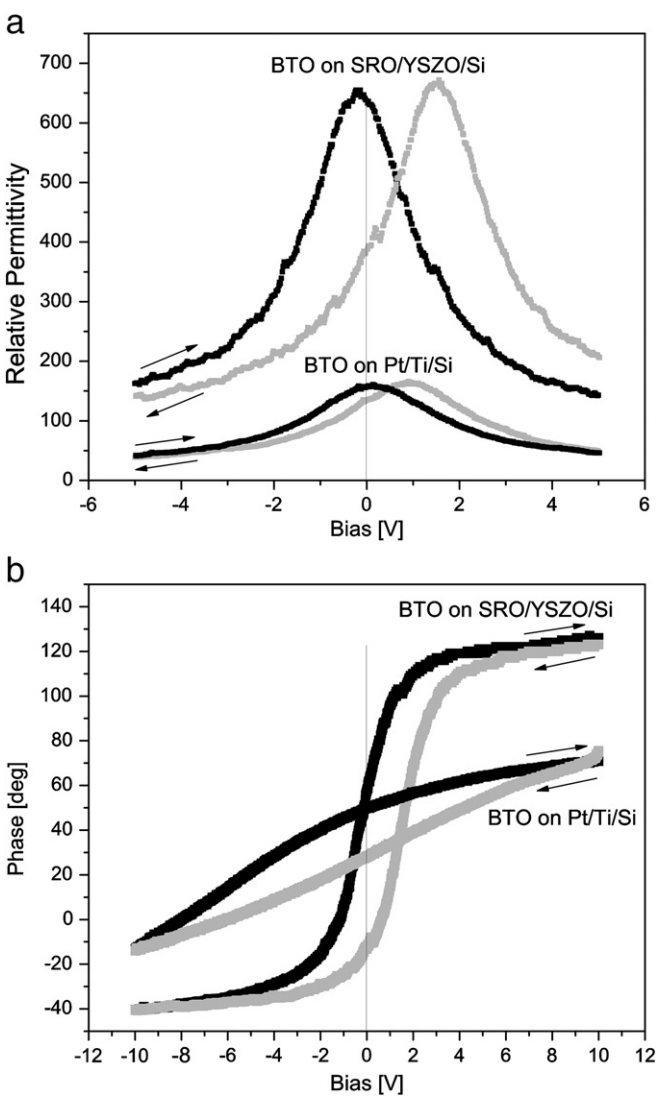

Fig. 7. a) *C–V* data of BTO films fabricated by multi-layer deposition and processed by one-step annealing at 800 °C. BTO/SRO/YSZO/Si and BTO/Pt/Ti/Si; b) Piezoresponse force microscopy (PFM) loops of the same films.

The local piezoelectric/ferroelectric properties of films were measured using PFM. Due to the considerable roughness of the film surface, the effect of domain switching could not be visualized by "domain-writing" with the PFM tip. However, local piezoresponse loops could be obtained easily, as shown in Fig. 7B. The data demonstrate that a domain structure exists and domain switching takes place. The phase difference between applied AC signal and piezoresponse is determined by the orientation of the local ferroelectric polarization in the sample. The obtained signal as a function of DC bias between sample and tip resembles *polarization–voltage* (*P–V*) hysteresis loops. Values obtained from the phase axis cannot be translated easily to actual polarization values (and hence to remnant polarization), but coercive field values correspond approximately to those found in *P–V* measurements. It can be seen in Fig. 7B that the BTO/SRO/YSZO/Si film exhibited very good piezoresponse properties, with a coercive field of 48 kV/cm, compared to 120 kV/cm and poor piezoresponse for the BTO/Pt/Ti/Si film. The increase of the coercive field in the latter case can be related directly to the presence of a non-ferroelectric, non-conductive silicate layer at the interface with BTO [35,36].

At the interface between BTO and SRO a transition layer was found by XPS that was not visible by FE-SEM. The influence of an interfacial layer on the dielectric properties of a barium titanate capacitor can be evaluated in terms of the well-established metal–ferroelectric–metal model [37], in which the total capacity is expressed in terms of the capacity of the BTO-based capacitor C_0, and the interface-based capacitors C_{i1} and C_{i2}, in series:

$$\frac{1}{C} = \frac{1}{C_{i1}} + \frac{1}{C_{i2}} + \frac{1}{C_0}. \quad (1)$$

Here C is the total capacity, C_{i1} is the capacity of the interface at the dielectric-lower electrode-interface, and C_{i2} is the corresponding capacity at the interface with the upper electrode. It is easily shown that for any finite value of C_{i1} or C_{i2}, the overall capacitance $C < C_0$. Hence, the interface acts as a dead layer that deteriorates the dielectric properties of the BTO film. It is known that epitaxial perovskite–perovskite interfaces such as the BTO/SRO interface provide superior dead-layer-originating capacities, close to the theoretical limit [37]. Nonetheless, it has also been demonstrated that mixing between SrO and BaO occurred at the $SrRuO_3$/BTO interface on a $SrTiO_3$(001) substrate. A complex interface is thus formed, even with well-defined surfaces and epitaxial films of two perovskites [38]. The formation of a dead layer at the interface with the bottom Pt or SRO electrode is therefore also expected in relatively imperfect polycrystalline BTO sol–gel films.

The influence of the upper electrode/BTO interface on dielectric properties is also important. Sputtering at low temperature is known to yield defects in the metal electrode microstructure, impeding conductivity. The difference in processing temperatures of bottom and top electrodes, and the different work functions of the two materials are likely to result in Schottky contact formation. That could also explain the asymmetric position of the *C–V* dependence with respect to 0 V bias (Fig. 7A).

Bulk strontium ruthenate is thermally stable up to 900 °C at ambient oxygen partial pressure [39]. Stable surfaces of $SrRuO_3$ have been reported up to at least 700 °C in oxygen/ozone atmospheres [26]. The stability at higher temperatures was not reported. On the other hand, $SrRuO_3$ exposed to oxygen/ozone, but post-annealed in vacuum formed Ru^0 and Sr_2RuO_4 [26]. The loss of ruthenium was due to formation of gaseous RuO_4. Our data show that the $SrRuO_3$ surface is unstable at 800 °C, and a small amount of what seems to be RuO_3 was detected in the film near the upper interface with BTO. When SRO is processed under vacuum, Sr-rich ruthenates, $Sr_{n+1}Ru_nO_{3n+1}$, containing partially reduced Ru are formed [26,40]. In our experiments the loss of Ru probably did not lead to quantitative amounts of $Sr_{n+1}Ru_nO_{3n+1}$ phases, as

XRD only showed the presence of oriented $SrRuO_3$. Loss of Ru therefore seems to be limited to the surface layer.

Processing of sol–gel derived BTO films on Pt/Ti/Si substrate led to a number of undesired effects. Titanium is a popular adhesion layer for platinizing Si/SiO_2 wafers [41]. It is known that annealing at ambient oxygen partial pressure leads to oxygen diffusion through Pt grain boundaries, partial oxidation of Ti to TiO_{2-x}, and migration of titanium dioxide to Pt [41]. Apparently, the reactivity of these phases at 800 °C is high, leading to diffusion of Si to Pt, and to platinum silicide formation. The Pt–Si binary system includes a number of phases, such as PtSi and Pt_6Si_5, that both match the stoichiometry found by XPS [42]. It is known that titanium dioxide can diffuse through platinum to the surface of an electrode at high temperature [41]. The XPS spectra showed that both Pt and Si were present in reduced form in the Pt-based electrode, whereas Ti was present in oxidized form. The formation of a silicide phase presented no practical problem, since the measured conductivity of the platinum silicide electrode was only 4% lower than that of pure Pt.

Silicate formation was shown to occur in these films within a minute at 800 °C. Due to the presence of silicon on the surface of the electrode, a Ba–Ti-silicate phase nucleated directly at the interface, and grew upon heat treatment. Under the assumption that the interfacial capacitance of the top electrode and the capacitance of the BTO layer were the same in both investigated capacitor architectures, it can be estimated that the 20 nm interfacial silicate layer has a relative permittivity of approximately 20. This value is in good agreement with values reported in literature for bulk fresnoite [34].

Decreasing the crystallization temperature of $BaTiO_3$ to below 650 °C could possibly prevent silicate phase formation, even if PtSi had formed. However, reduced processing temperatures will also affect the morphology of the BTO film. It has been demonstrated that the dielectric properties depend strongly on processing temperature, and 650 °C was found to be insufficient to obtain high relative permittivities [8,9]. The poor performance of $BaTiO_3$ at low processing temperatures is related to the stability of the oxocarbonate phase $Ba_2Ti_2O_5CO_3$, which shifts the onset of perovskite phase formation to 600–650 °C. It has been shown that the crystallization temperature of barium strontium titanate films can be decreased to 500 °C, but these films were obtained from a non-alkoxide–carboxylate process involving the processing of metallic Ba and Sr [43]. Furthermore, stable hydroxyl defects in the structure are known to stabilize the non-ferroelectric cubic phase instead of the high-*k* tetragonal phase at room temperature. The unit cell of the cubic phase is larger than that of the defect-free tetragonal phase [2,44,45]. High temperature processing leads to removal of hydroxyl defects, but the high density of hydrothermal $BaTiO_3$ is retained only above 800 °C [45]. This is due to the fact that removal of hydroxyl defects leads to formation of thermodynamically stable internal pores in barium titanate grains. Both hydroxyl defects and internal porosity lead to a loss of dielectric properties, unless it is processed at sufficiently high temperatures [44,45].

4. Conclusions

The formation of silicates such as fresnoite at the interface between barium titanate and platinum silicide leads to formation of a dead layer of very low relative permittivity (*ca.* 20). The existence of the interface degenerates the dielectric properties of barium titanate based capacitors, leading to a considerable decrease of relative permittivity. The problem is related to high-temperature processing of dense sol–gel-derived films of barium titanate by rapid thermal annealing and multi-layer deposition. As long as a high annealing temperature is necessary to obtain the desired dielectric properties, the problem of Si diffusion and silicate interface formation can be solved by the use of $SrRuO_3$ electrodes with a ZrO_2–x%Y_2O_3 buffer film between the electrode and the silicon substrate.

References

[1] D. Yoon, J. Ceram. Proc. Res. 7 (2006) 343.
[2] C. Pithan, D.H. Hennings, R. Waser, Int. J. Appl. Ceram. Technol. 2 (2005) 1.
[3] R.W. Schwartz, T.S. Schneller, R. Waser, C. R. Chimie 7 (2004) 433.
[4] R.W. Schwartz, in: D.B. Mitzi (Ed.), Solution Processing of Inorganic Materials, John Wiley & Sons Inc, New Jersey, 2009, p. 33.
[5] M. Huffman, Integr. Ferroelectr. 10 (1995) 39.
[6] H. Schroeder, A. Kingon, in: R. Waser (Ed.), Nanoelectronics and Information Technology: Advanced Electronic Materials and Novel Devices, Wiley VCH GmbH & Co, Weinheim, 2003, p. 540.
[7] J.F. Scott, C.A. Paz de Araujo, Science 246 (1989) 1400.
[8] U. Hasenkox, S. Hoffmann, R. Waser, Sci. Technol. 12 (1998) 67.
[9] S. Hoffmann, R. Waser, J. Europ. Ceram. Soc. 19 (1999) 1339.
[10] P.P. Phule, S.H. Risbud, Adv. Ceram. Mater. 3 (1988) 183.
[11] R.W. Schwartz, Chem. Mater. 9 (1997) 2325.
[12] M.H. Frey, D.A. Payne, Chem. Mater. 7 (1995) 123.
[13] A. Mosset, I. Gautier-Luneau, J. Galy, P. Strehlow, H. Schmidt, J. Non-Cryst. Solids 100 (1988) 339.
[14] R.W. Schwartz, P.G. Clem, J.A. Voigt, E.R. Byhoff, M. van Stry, T.J. Headley, N.A. Missert, J. Am. Ceram. Soc. 82 (1999) 2359.
[15] K.J. Hubbard, D.G. Schlom, J. Mater. Res. 11 (1996) 2757.
[16] M.D. Nguyen, K. Karakaya, P.M. te Riele, D.H.A. Blank, A.J.H.M. Rijnders, In: Proceedings of the Third IEEE-NEMS, 6–9 January 2008, Sanya, China, p. 315.
[17] M. Dekkers, M.D. Nguyen, R. Steenwelle, P.M. te Riele, D.H.A. Blank, G. Rijnders, Appl. Phys. Lett. 95 (2009) 012902 (1–3).
[18] S.J. Wang, C.K. Ong, L.P. You, S.Y. Xu, Semicond. Sci. Technol. 15 (2000) 836.
[19] W.S.M. Werner, W. Smekal, C.J. Powell, NIST Datanase for the Simulation of Electron Spectra for Surface Analysis, National Institute of Standards and Technology, Gaithersburg, 2006.
[20] T.M. Stawski, S.A. Veldhuis, O.F. Göbel, J.E. ten Elshof, D.H.A. Blank, J. Am. Ceram. Soc. 93 (2010) 3443.
[21] B. Carriere, J.P. Deville, D. Brion, J. Escard, J. Electron. Spectrosc. Relat. Phenom. 10 (1977) 85.
[22] P.J. Grunthaner, F.J. Grunthaner, A. Madhukar, J. Vac. Sci. Technol. 20 (1982) 680.
[23] W. Göpel, J.A. Anderson, D. Frankel, M. Jaenig, K. Phillips, J.A. Schäffer, G. Rocker, Surf. Sci. 139 (1984) 333.
[24] C.C. Hung, R.E. Riman, R. Caracciolo, Ceram. Trans. 12 (1990) 17.
[25] T.P. Nguyen, S. Lefrant, J. Phys. Condens. Matter 1 (1989) 5197.
[26] J. Shin, S.V. Kalinin, H.N. Lee, H.M. Christen, R.G. Moore, E.W. Plummer, A.P. Baddorf, Surf. Sci. 581 (2005) 118.
[27] M.V. Rama Rao, V.G. Sathe, D. Sornadurai, B. Panigrahi, T. Shripathi, J. Phys. Chem. Solids 61 (2000) 1989.
[28] P.A. Cox, R.G. Egdell, J.B. Goodenough, A. Hamnett, C.C. Naish, J. Phys. C 16 (1983) 6221.
[29] D.D. Sarma, C.N.R. Rao, J. Electron. Spectrosc. Relat. Phenom. 20 (1980) 25.
[30] K.S. Kim, N. Winograd, J. Catal. 35 (1974) 66.
[31] H.J. Lewrenz, S. Stucki, R. Kötz, Surf. Sci. 126 (1983) 463.
[32] R.P. Vasquez, J. Electron. Spetrosc. 56 (1991) 217.
[33] PDF 00-022-0513. International Centre for Diffraction Data 2005.
[34] B. Rangarajan, T. Shrout, M. Lanagan, J. Am. Ceram. Soc. 92 (2009) 2642.
[35] A.K. Tagantsev, I.A. Stolichnov, Appl. Phys. Lett. 83 (2003) 3356.
[36] N.A. Pertsev, J. Rodriguez Contreras, V.G. Kukhar, B. Hermanns, H. Hohlstedt, R. Waser, Appl. Phys. Lett. 74 (1999) 1326.
[37] M. Stengel, N.A. Spaldin, Nature 443 (2006) 679.
[38] J. Shin, A.Y. Borisevich, V. Meunier, J. Zhou, E.W. Plummer, S.V. Kalinin, A.P. Baddorf, ACS Nano 4 (2010) 4190.
[39] W. Bensch, H.W. Schmalle, A. Reller, Solid State Ionics 43 (1990) 171.
[40] C. Mallika, O.M. Sreedharan, J. Alloys Compd. 191 (1993) 219.
[41] K. Sreenivas, I. Reaney, T. Maeder, N. Setter, C. Jagadish, R.G. Elliman, J. Appl. Phys. 75 (1994) 232.
[42] L.E. Tanner, H. Okamoto, J. Phase Equilib. 12 (1991) 571.
[43] S. Halder, T. Schneller, R. Waser, Sci. Technol. 33 (2005) 299.
[44] M.H. Frey, D.A. Payne, Phys. Rev. B 54 (1996) 3158.
[45] D.F.K. Hennings, C. Metzmacher, B.S. Schreinemacher, J. Am. Ceram. Soc. 84 (2001) 179.